Momentum distribution of photoelectrons emitted from Cu and Ag single crystals, and its polarization dependence*

H. Becker, E. Dietz, U. Gerhardt, and H. Angermüller

Physikalisches Institut der Universität Frankfurt, D-6 Frankfurt am Main, Germany

(Received 30 December 1974)

The angular-resolved energy-distribution functions for photoelectrons emitted from (111) Cu and Ag are presented at photon energies below 6.2 eV. They show a characteristic dependence on the polarization of the radiation in spite of the fact that the experiments are done at normal incidence. No such polarization dependence is observed for (110) and (001) Cu surfaces. The polarization dependence is traced to the angular dependence of the dipole matrix element characteristic for direct transitions; it allows one to separate the elastically emitted electrons from those emitted after being scattered. An interpolation scheme is used to calculate $E(\vec{k})$ consistent with the experiments of this paper and with independent optical and de Haas–van Alphen measurements. The nearly-free-electron case is used as a guide in the interpretation, it reveals only qualitative similarities with the actual experiments.

I. INTRODUCTION

Photoemission experiments are frequently used in solid state spectroscopy. In most cases, the energy distribution $N(E)$ of all electrons emitted from a polycrystalline sample is measured for several photon energies irrespective of the direction of emission. Neglecting the contribution of scattered electrons, $N(E)$ contains information about the absolute energy position of the initial and final states cooperating in the excitation process. The optical constants, on the other hand, contain information only about the energy differences between the final and initial states. This advantage of $N(E)$ compared to the optical constants is partially offset by the fact that there is no clearcut way to distinguish in $N(E)$ the elastically emitted electrons from those scattered in the volume or at the surface of the sample. Since both $N(E)$ and the optical constants are given by the sum over many individual processes, the problem of sorting out the various different contributions arises in both cases.

Consider, by contrast, the momentum distribution of photoelectrons, i.e., their energy and angular distribution. In particular, we concentrate in our investigation on the momentum distribution for normal incidence of the radiation onto single crystalline surfaces of various orientations. We also assume that it is somehow possible to single out the elastically emitted photoelectrons. The measured quantity is given by one particular excitation process in this case, i.e., the investigation of the momentum distribution probes these individual processes directly. It is therefore a better way of doing solid state spectroscopy than the investigation either of the optical constants or of $N(E)$. At the same time it is more demanding experimentally, which is the reason that there are only a few measurements of this kind.[1,2]

The problem in analyzing the momentum distribution is, of course, how to single out the elastically emitted electrons. Gobeli, Allen, and Kane[1] showed how to solve this problem. They investigated and analyzed how the angular distribution of photoelectrons emitted from Ge and Si (111) surfaces depends on the polarization of the incident radiation. Their analysis is based on the three-step model of photoemission[3] which will be described below. It is important to note that this polarization dependence is *not* the one described by Fresnel's equations, since the experiment was done with normal incidence of the exciting radiation. One might wonder why there is a polarization dependence at all for cubic crystals like Ge and Si which are optically isotropic. Consider a direct transition with reduced wave vector $\vec{k}_0$. Acting on $\vec{k}_0$ with all symmetry elements of the crystal generates the star of $\vec{k}_0$ with the arms $\vec{k}_0, \ldots, \vec{k}_i, \ldots, \vec{k}_n$. All direct transitions with the different $\vec{k}_i$ are energetically degenerate and thus contribute to the optical absorption. The occupancy of a given final state $E_{n'}(\vec{k}_i)$ is proportional to $|\langle n\vec{k}_i | \vec{A} \cdot \vec{p} | n'\vec{k}_i \rangle|^2$ and is thus strongly dependent on the orientation of the vector potential $\vec{A}$ of the radiation. In calculating the optical absorption we have to sum the contributions from all arms of the star, and this *sum* turns out to be isotropic for cubic crystals. Since the momentum distribution of the photoelectrons probes individual transitions, e. g., the direct transition with $\vec{k} = \vec{k}_i$, it is obvious that it should depend strongly on the orientation of $\vec{A}$ with respect to the crystal axes even for normal incidence of the light.

The model used by Gobeli, Allen, and Kane assumes that the photoemission process can be described by the succession of three independent steps, namely, (i) direct $\vec{k}$-conserving band-to-band transitions in the volume of the crystal, (ii) transport of the excited electron to the surface,

(iii) transmission of the excited electron through the surface into the vacuum.[3] The third step is equivalent to momentum and energy conservation in the low-energy-electron-diffraction (LEED) case. In both cases the *reduced* wave vector $\vec{k}_t$ in the surface must be conserved since there is translational symmetry in the ideal surface and thus the tangential vector $\vec{k}_t$ is a good quantum number. Since $\vec{k}_t$ is a reduced wave vector in the usual sense, reciprocal surface lattice vectors may be added corresponding to the different orders of diffraction. There is no translational symmetry normal to the surface, i.e., the normal component of $\vec{k}$ is not conserved and will change during the transmission or reflection in order to allow for energy conservation.

While the three-step model seems to be a natural approximation to the photoemission process, it is not necessarily the adequate model in all cases. As a matter of fact, the discussion about the proper model to describe photoemission started right at the beginning of solid state physics. It was argued that a model describing the optical absorption properly might not be the correct starting point for photoemission since electrons excited just at the surface have the highest escape probability. Thus the optical absorption which is made possible by the steplike potential at the surface, while contributing very little to the optical constants, might be important in photoemission.[4] The significance of this surface effect is still under debate.[5] The surface absorption vanishes if the electric field of the radiation has no component normal to the surface. Since we use normal incidence of the exciting radiation and assume that the surfaces of our crystals are smooth, the surface effect will not contribute in our case. Surface states might also contribute to photoemission from metals.[6] However, we have found no clues for these effects in Cu and Ag at low photon energies and will therefore neglect them.

The three-step model is most likely to hold at low energies where the mean free path of the excited electrons is highest.[3,7] The assumption of direct transitions between Bloch states undisturbed by the surface should be a good approximation in this region. Thus we use the near-ultraviolet spectral region to measure the momentum distribution of the photoelectrons emitted from Cu and Ag single crystals and analyze the results in terms of the three-step model. Our aim is to compare the spectroscopic information thus obtained with the calculated energy bands which are consistent with independent experiments. This procedure constitutes a rigorous test of the three-step model in the low-energy region. Our choice of the materials is partly motivated by the fact that the band structure of these "model d-band metals"

is known with a reasonable accuracy. Furthermore, preliminary measurements on Cu showed a sizable fraction of the photoelectrons to be emitted without scattering.[2] Experimentally, the possibility to generate high-quality surfaces epitaxially and by electropolishing is also advantageous.

In Sec. II, we describe the experimental procedures and present the experimental results. Thereafter, we discuss the consequences of the three-step model for the momentum distribution and its polarization dependence for the case of nearly free electrons. Finally, we analyze the experimental results in terms of the band structure of Cu and Ag and present the consequences of this analysis.

II. EXPERIMENTS: METHODS AND RESULTS

Light emitted from a H_2 hot-filament arc discharge passes through a grating monochromator and a polarizer consisting of a dichroitic film supported by a fused quartz substrate.[8] The two extremal positions of the polarizer subtend $\pm 45°$ with respect to the slits of the monochromator. The intensity of the beam leaving the polarizer is thus nearly the same for the two positions, in spite of the fact that the monochromator produces partially polarized light. Any remaining differences in the intensities, monitored by measuring the luminescence of a sodium salicylate layer with a photomultiplier tube, are compensated by inserting a fused quartz plate into the beam. The plate is tilted until the intensities for the two positions of the polarizer differ by less than $\pm 0.5\%$. Fused quartz lenses are used to focus the light onto the entrance slit of the monochromator and onto the sample. The monochromator is usually operated at a resolution of 0.13-eV full width at half-maximum (FWHM).

The electron analyzer and the data acquisition system are shown schematically in Fig. 1. The analyzer is located inside a stainless-steel ultrahigh vacuum chamber evacuated by a 400-liter/sec electrostatic ion pump. The operating pressure after mild bakeout is 10^{-9} Torr. A μ-metal shield reduces the magnetic field at the analyzer to values below 0.05 G, corresponding to a deflection below 1 mm at the windows of the analyzer for photoelectrons with $E = 0.1$ eV. The angular distortion induced by the residual magnetic field is thus small compared to the angular resolution for electron energies above 0.1 eV. The light enters the vacuum chamber through a sapphire window, the optical axes of which are orientated parallel and perpendicular to the polarizer, respectively. The light beam which hits the sample at normal incidence has an aperture of 5×10^{-3} sr, its diameter at the sample is 3 mm.
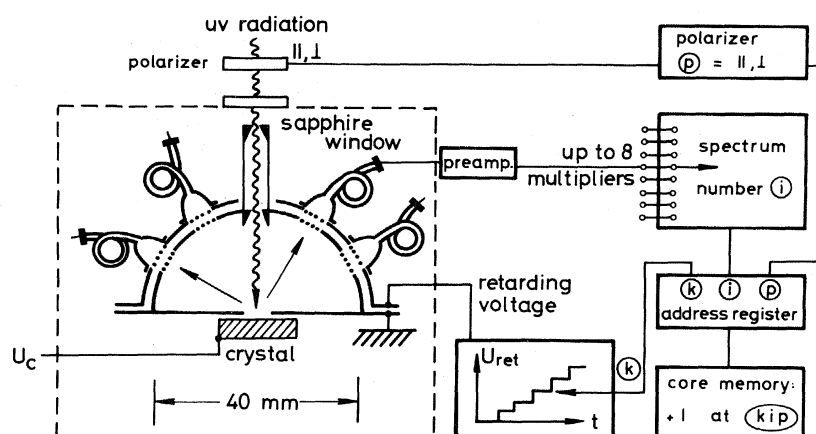
The light beam is parallel to the polar axis of

FIG. 1. Energy analyzer and data acquisition system, both shown schematically.

two concentric hemispheres of 40 and 44 mm diameter, respectively, which are fabricated from 0.5-mm sheet copper. Photoelectrons emitted from the single crystalline surface which is situated at the center of the hemispheres travel through a field free region. This region is provided by the inner hemisphere and by a 0.5-mm-thick copper disk in the equatorial plane. The disk has a bore 10 mm in diameter concentric to the polar axis. Both the disk and the inner hemisphere are at ground potential. Possible contact potentials between the sample and the analyzer are compensated by applying the proper voltage to the sample.

The hemispheres are equipped with concentric holes of 5 mm diameter to allow observation of the emitted electrons for various fixed angles of emission. The angular resolution is thus $\pm 10°$, taking the finite cross section of the light beam into account. The holes are covered with copper grids of 33-μm mesh size. The photoelectrons are detected by six channel electron multipliers[9] while the energy analysis is accomplished by applying a steplike retarding voltage to the outer hemisphere. The cathode of such a multiplier is shaped like a funnel. The rim of the funnel is made of platinum which is sealed directly to the glass tubing of the multiplier and is thus in contact with the high resistivity coating on its inside. The field distribution inside of the funnel assures that virtually all electrons transmitted through the observation window of the outer hemisphere are detected. The glass tubing is closed at the anode side, since the multipliers are operated in the pulse counting mode only. The anode itself consists of a platinum wire sealed to the tubing. The leads from the different anodes to the electrical feedthrough are shorter than 100 mm. Simple preamplifiers[9] situated at the atmospheric side of the feedthroughs boost the output pulses of the multipliers to +5-V amplitude and 1-μsec duration. No crosstalk occurs between different signal channels. The number of pulses

produced by ions originating from the ion pump is reduced to about 10 cps by means of an electrostatic shield.

The data acquisition system, also shown in Fig. 1, is organized as follows. At the instant at which one of the multipliers, e.g., multiplier number i supplies an output pulse, this number and simultaneously the number of the particular step in the retarding voltage, say, k and the position of the polarizer p are transmitted to the address register of a multichannel analyzer. Thereafter, one count is added to the address ikp of the core memory. Arriving at the highest preselected retarding voltage, the polarizer is turned by 90° and the retarding voltage returned to its lowest value. The dwell time on one step of the retarding voltage is 1 sec. Typically, 10^4 to 10^5 counts are accumulated in one particular cell ikp of the core memory within 10 h. The energy-distribution function for photoelectrons emitted into the different windows of observation i for the orientation p of the polarizer is obtained by differentiating the spectrum ip which is a function of the retarding voltage specified by k.

Two different methods are used to prepare the samples. In the case of copper, the desired surface orientation is produced by cutting a bulk single crystal with an annular diamond saw running at one revolution per second and using a load below 0.2 N/cm. After grinding with waterproof silicon carbide paper, the sample is annealed in a H_2 atmosphere at 700 °C for 30 min and its orientation checked by means of a Laue diagram. Finally, the surface is electropolished in orthophosphoric acid,[10] rinsed in alcohol and quickly transferred to the vacuum system. Surfaces thus prepared show a sharp LEED pattern even without annealing. The silver (111) surfaces, on the other hand, were grown epitaxially on mica substrates in another ultrahigh vacuum chamber and then transferred. In both cases the sample is annealed together with
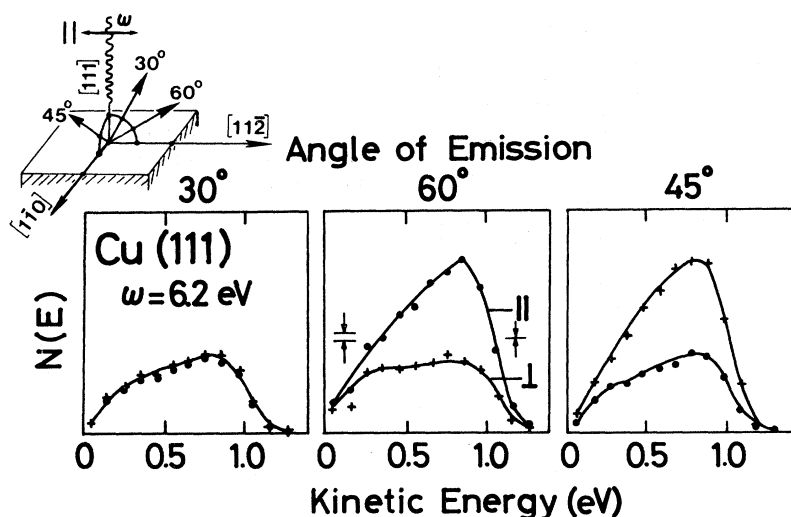
FIG. 2. Angular and energy distribution of photoelectrons emitted from a (111) Cu surface for two polarizations of the radiation at $\omega = 6.2$ eV. The directions of observation are also indicated. The symbols ‖ and ⊥ refer to the vector potential of the radiation orientated parallel and perpendicular to the mirror plane $(1\bar{1}0)$ which is the plane of emission for 30° and 60°. Each function is actually the average of two simultaneous measurements in the same plane of emission, but on either side of the surface normal. They are normalized to the same maximum of the perpendicular polarization.

the analyser at about 250 °C for several hours.

The experimental results for the angular and energy distribution of photoelectrons emitted from a (111) Cu surface for two polarizations of the radiation with $h\nu = \omega = 6.2$ eV are presented in Fig. 2. The insert shows the orientation of the windows of observation. The 30° and 60° direction with respect to the surface normal lie in the $(1\bar{1}0)$ mirror plane, while the 45° direction is in the $(11\bar{2})$ plane which is perpendicular to $(1\bar{1}0)$. The symbols ‖ and ⊥ refer to the electric field vector of the exciting radiation parallel and perpendicular to $(1\bar{1}0)$, respectively. The curves give the kinetic energy distribution functions $N(E)$ for three directions of emission and two positions of the polarizer. The number of emitted electrons with kinetic energies between E and $E + dE$ is $N(E)dE$, as usual. There is evidently no polarization effect for 30°, while $N(E)_{\parallel}$ and $N(E)_{\perp}$ differ drastically for 45° and 60°.

The functions given in Fig. 2 are actually already normalized and averaged in a way which we shall use also in Figs. 4 and 5. We explain this procedure in reference to Fig. 3 containing the original experimental curves for Cu(111) at $\omega = 6.2$ eV. The two spectra shown for each angle of emission and each polarization belong to directions to the left and to the right of the surface normal in the planes specified above, i.e., $(1\bar{1}0)$ for 30° and 60° and $(11\bar{2})$ for 45°. Since the two 45° directions lie on either side of the mirror plane $(1\bar{1}0)$, the two functions have to be identical for each polarization. This is borne out by our measurements within the experimental uncertainty. There is no mirror symmetry for the 30° and 60° pairs. However,

•as we shall discuss below, $E(k)$ for Cu and Ag shows an approximate rotational symmetry around the [111] axis. Since the experimentally observed differences are insignificant, we average over the respective pairs for the different angles of emission and for the two polarizations in order to increase the signal-to-noise ratio. Furthermore, we normalize the results to the same value of the maximum in $N(E)_{\perp}$, since the variation of the quantum efficiency of the different multipliers which is about $\pm 30\%$ is of the same order of magnitude as the variation in the maximum value of $N(E)_{\perp}$. This normalization is also advantageous in the analysis of the experimental data. The normalization and
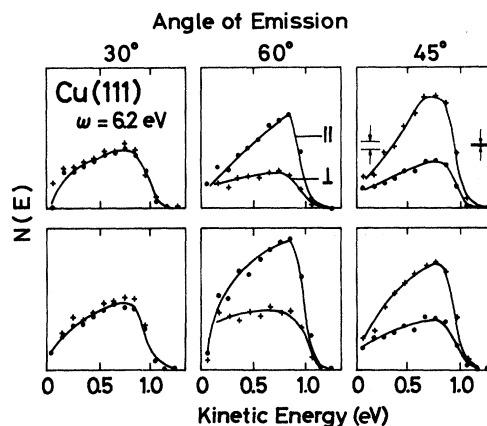

FIG. 3. Original measurements of the angular and energy distribution and their dependence on the polarization for Cu(111), $\omega = 6.2$ eV. These curves are averaged and normalized to produce the functions previously shown in Fig. 2.

averaging procedure condenses the original experimental data of Fig. 3 to the results presented in Fig. 2.

The polarization effects apparent in Figs. 2 and 3 will be used to identify unscattered photoelectrons. We therefore plot $N(E)_\parallel - N(E)_\perp$ for Cu(111) in Fig. 4, determined at three different photon energies and three angles of emission. The curves are normalized and averaged as described above. Actually, $N(E)_\perp - N(E)_\parallel$ is plotted for 45° since $\parallel$ and $\perp$ refer to (1$\bar{1}$0) and not to (11$\bar{2}$) which is the plane of emission for 45°. The corresponding results for Ag(111) plotted in the same fashion are shown in Fig. 5 for four different photon energies. Our analysis will center on the curves presented in Figs. 4 and 5. However, there are other important experimental results. We find no polarization effect for a polycrystalline Cu film. This confirms that the intensity of the radiation impinging on the sample is indeed identical for the two polarizations. More important, we also find $N(E)_\parallel - N(E)_\perp$ = 0 for Cu(110) and (001) surfaces at all photon energies between 4.8 and 6.2 eV, in spite of the same surface preparation techniques as used for Cu(111). The size of the polarization effect for Cu(111) depends drastically on the perfection of the surface, it increases with the annealing time and decreases to zero after exposure of the surface to atmospheric pressure for a few hours.

III. PREDICTIONS FOR NEARLY FREE ELECTRONS

Direct transitions for Cu and Ag occur between the sp bands for the spectral region of our experiments. These bands show some similarity to nearly-free-electron bands, in contrast to the more localized d levels below the Fermi energy E_F which have tight-binding character. However,

FIG. 5. Polarization effect for emission from Ag(111) at various photon energies. As in Fig. 4, the difference in the energy distribution functions for polarization parallel and perpendicular to the plane of emission is plotted.

since the sp bands interact strongly with the d bands, any attempt to analyze the data *quantitatively* in terms of nearly-free-electron bands neglecting or including the gap at the zone boundary fails. This interaction is apparent in Fig. 6 which shows the band structure of Cu.[11] The transitions of interest occur in the neighborhood of the $L_1 - L_{2'}$ gap. Although the $L_{2'}$ eigenvalue is close to nearly-free-electron energy shown by the dashed lines, the corresponding value for L_1 above $L_{2'}$ is not. There is obviously a strong interaction of this L_1 level with the L_1 level in the d bands below E_F while there is no such interaction for $L_{2'}$ since a level of this symmetry is missing in the d bands. The asymmetric splitting of the $L_1 - L_{2'}$ gap is not described by a two-band model, nor is the strong nonparabolic dependence of the bands starting at
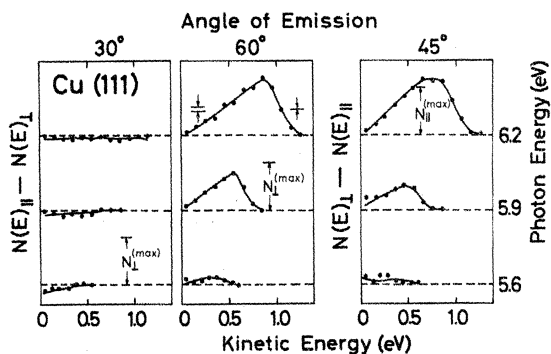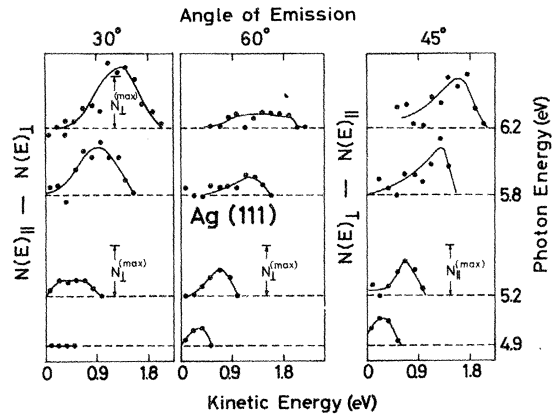

FIG. 4. Difference in the angular resolved energy distribution produced by changing the orientation of the polarizer for photoelectrons emitted from Cu(111) at various photon energies. Plotted is the difference in the energy distribution functions measured with the polarizer parallel and perpendicular to the plane of emission, respectively.
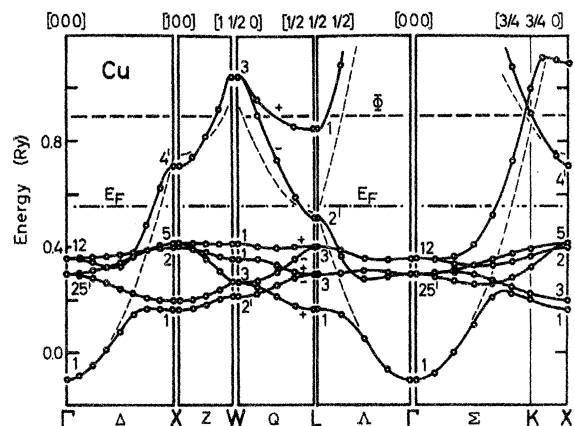

FIG. 6. Band structure of Cu as calculated by Segall and Burdick (Ref. 11). The dashed curves are the free-electron eigenvalues. The position of the Fermi energy E_F and of the work function Φ is also given.

L_1 and $L_{2'}$.

In spite of the warnings given above, we go ahead nonetheless to discuss the results expected for nearly free electrons (NFE),[12] since they show the proper *qualitative* trends and since this is the easiest way to explain our method of analysis. For the initial state $|n\vec{k}\rangle$ and the final state $|n'\vec{k}\rangle$ we write

$$E_n(\vec{k}) = \frac{\hbar^2}{2m}(\vec{k} + \vec{g})^2 \equiv (\vec{k} + \vec{G})^2, \quad |n\vec{k}\rangle = e^{i(\vec{k}+\vec{g})\cdot\vec{r}}\left(1 + \sum_{\nu \neq 0} \frac{V_{G\nu}}{(\vec{k}+\vec{G})^2 - (\vec{k}+\vec{G}+\vec{G}_\nu)^2} e^{i\vec{g}_\nu\cdot\vec{r}}\right);$$

$$E_{n'}(\vec{k}) = \frac{\hbar^2}{2m}\kappa^2 \equiv k^2 = k_a^2 + k_t^2, \quad |n'\vec{k}\rangle = e^{i\vec{\kappa}\cdot\vec{r}}\left(1 + \sum_{\nu \neq 0} \frac{V_{G\nu}}{k^2 - (\vec{k}+\vec{G}_\nu)^2} e^{i\vec{g}_\nu\cdot\vec{r}}\right).$$

(1)

The dipole matrix element between these states is proportional to

$$\langle n\vec{k}|\vec{p}|n'\vec{k}\rangle \propto \frac{V_G}{k^2 - (\vec{k}+\vec{G})^2}\vec{G} + \sum_{\nu \neq 0} \frac{V_G V_{G+G_\nu}}{[(\vec{k}+\vec{G})^2 - (\vec{k}+\vec{G}+\vec{G}_\nu)^2][\vec{k}^2 - (\vec{k}+\vec{G}+\vec{G}_\nu)^2]}(\vec{k}+\vec{G}+\vec{G}_\nu).$$

(2)

Energy and momentum conversation for the absorption process requires

$$h\nu \equiv \omega = E_{n'}(\vec{k}) - E_n(\vec{k}) = 2k_a G - G^2, \quad k_a > \tfrac{1}{2}G,$$

(3)

which shows that the component k_a of $\vec{k}$ antiparallel to $\vec{G}$ depends only on the photon energy ω. The optical energy surface is thus a plane perpendicular to the reciprocal-lattice vector $\vec{G}$, it is given as the dashed-dotted line in Fig. 7. Also shown are the surfaces of constant initial and final energies, which are spheres with their centers displaced by $\vec{G}$. The vector $\vec{G}$ corresponds to $(2\pi/a)(-1, -1, -1)$ for the low-energy transitions in Cu and Ag. The crystal surface shown in Fig. 7 perpendicular to $\vec{G}$ thus corresponds to a (111) surface orientation for which we observe the strong polarization effects in Cu and Ag. We discuss the momentum distribution of the photoelectrons in the NFE model for this special surface orientation only. We also disregard diffraction at the surface since the diffracted electrons are not allowed to leave the crystal by energy conservation at the low energies typical for our experiments. Energy conservation and conservation of the tangential component $\vec{k}_t$ of $\vec{k}$ requires for the emission process

$$E = k_v^2 + k_t^2 = E_{n'} - (E_F + \Phi) = \frac{(G^2 + \omega)^2}{4G^2} + k_t^2 - (E_F + \Phi)$$

or

(4)

$$E\cos^2\vartheta = k_v^2 = \frac{(G^2 + \omega)^2}{4G^2} - (E_F + \Phi),$$

where E is the kinetic energy of the electron in vacuum and Φ is the work function. For emission to occur k_v has to be real or $k_v^2 \geq 0$. The smallest photon energy for which emission is possible is therefore given by

$$\omega_{\min} = 2G(E_F + \Phi)^{1/2} - G^2,$$

(5)

which is to be compared with $\omega_0 = \Phi$ for a polycrystalline sample. The kinetic energy is restricted to the range

$$k_v^2 \leq E \leq \omega - \Phi.$$

(6)

The upper limit corresponds to $E_n(\vec{k}) = E_F$, it restricts the emission angle ϑ with respect to the surface normal to $\vartheta_{\max}$ with

$$\cos\vartheta_{\max} = k_v^2(\omega)/(\omega - \Phi).$$

(7)

Counting the number of states contributing to photoelectrons within the range of kinetic energies dE and the azimuthal range $d\phi$ for an exciting radiation with spectral width $d\omega$ results in

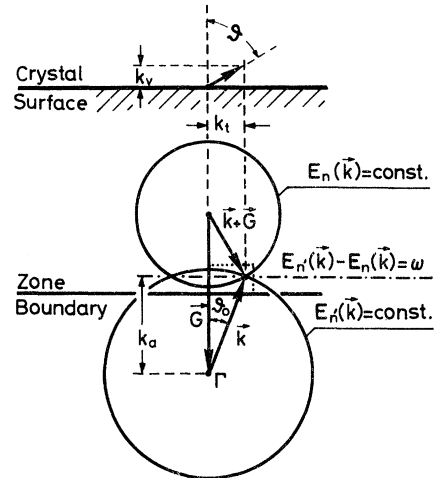$$dZ = [2V/(2\pi)^3](4G)^{-1} d\omega \, dE \, d\phi.$$

(8)

FIG. 7. Contours of constant energy for nearly free electrons, characterizing direct optical transitions. The subscripts n and n' refer to the initial and final states, respectively. The reciprocal-lattice vector $\vec{G}$ supplies the momentum necessary for momentum conservation in the optical transition. Energy conservation defines the optical energy contour $E_{n'} - E_n = \omega$ which is the dash-dotted line perpendicular to $\vec{G}$. The tangential component $\vec{k}_t$ of the wave vector $\vec{k}$ is conserved during the emission of a photoelectron.

Integrating over ϕ and taking Eq. (6) into account yields the familiar box structure for the NFE energy distribution function averaged over all directions of emission.[3,13]

For infinitely high angular and spectral resolution, the energy distribution for a given direction of emission would be a δ function, according to Eq. (4). Unfortunately, the intensity would be zero in this case, which shows that the finite angular and spectral resolution must be taken into account in analysing the experiments. For this purpose, we define a hypothetical NFE Cu by G^2 $= 36$ eV, $\Phi = 4.75$ eV, $E_F = 7.5$ eV, and $\omega_{min} = 6$ eV as given by Eq. (5). The NFE energy contours for these parameters are shown in Fig. 8 close to the L point in a plane containing $\vec{G} = (2\pi/a)(-1,-1,-1)$. The depicted region is indicated by the dotted rectangle in Fig. 7. For the initial states, only $E_n(\vec{k})$ $= E_F$ is given, while the final-state energy ranges from $E_{vac} = E_F + \Phi$ to 3 eV above E_{vac}. Three different photon energies, i.e., optical energy surfaces, are marked by dash-dotted lines. For $\omega = \Phi$, the finite tangential component k_t and $E = 0$ requires purely imaginary k_v, i.e., total internal reflection, in accordance with $\omega < \omega_{min}$. The shaded areas are the regions of $\vec{k}$ space contributing to emission for an angular resolution of $\pm 5°$. The boundaries of these areas for the average angle of emission $\bar{\vartheta} = 30°$, $45°$, and $60°$ are all tan-

FIG. 9. Angular resolved energy distribution functions calculated for the hypothetical NFE Cu of Fig. 8 at various photon energies ω. The finite width of the functions is generated mainly by the finite angular resolution of $\pm 7°$. The spectral resolution which is represented by a Gaussian of 0.13-eV full width at half-maximum has only a minor influence. The dotted rectangle is the box expected for the NFE energy distribution averaged over all directions of emission.
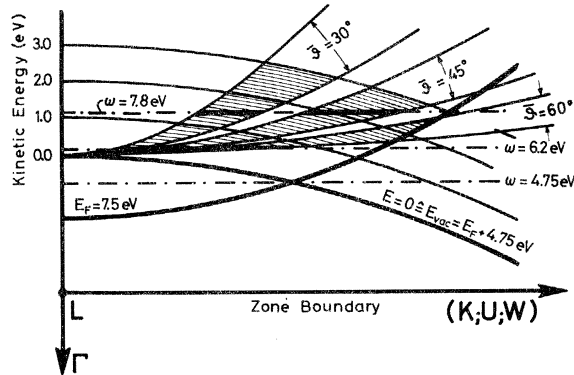

FIG. 8. Contours of constant energy for nearly free electrons in the neighborhood of the Brillouin-zone boundary. The region of $\vec{k}$ space depicted here is indicated by the dotted rectangle in Fig. 7. The contours are drawn for a hypothetical NFE Cu defined by $G^2 = 36$ eV, $\Phi = 4.75$ eV, and $E_F = 7.5$ eV. From the initial states, only the contour corresponding to the Fermi sphere is shown, while four contours of constant final energy are given. States within the three shaded areas will give rise to photoelectrons detected under 30°, 45°, and 60° to the surface normal, respectively, provided the surface normal is parallel to $\vec{G}$, as indicated in Fig. 7. The finite width of these areas stems from the finite angular resolution of the electron analyzer, assumed to be $\pm 5°$ in this case.
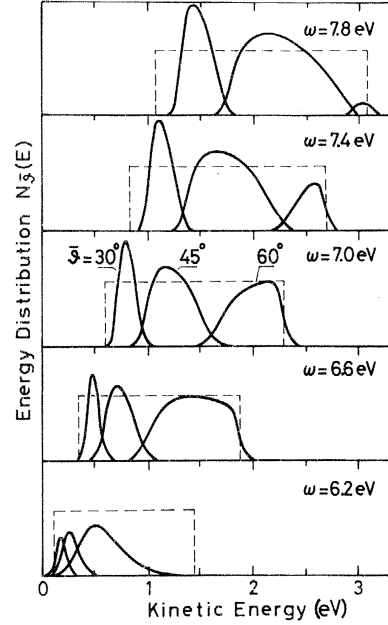
gential to $E_{n'}(\vec{k}) = E_{vac}$ and $\omega = \omega_{min}$ at the point where the [111] axis intersects these surfaces. The optical surface $\omega = 6.2$ eV cuts through all three regions, which means that a finite energy distribution will be observed for each $\bar{\vartheta}$. For ω $= 7.8$ eV, the optical surface runs through the region $\bar{\vartheta} = 60°$ outside of the Fermi sphere, i.e., emission will occur only for $\bar{\vartheta} = 30°$ and $\bar{\vartheta} = 45°$.

We calculate $N_{\bar{\vartheta}}(E)$ by numerically integrating the contributions

$$\frac{dZ}{dE} = dN_{\bar{\vartheta}} = \frac{V}{(2\pi)^3 2G} d\omega \, d\phi \qquad (9)$$

as derived from Eq. (8) using the angular resolution $\pm 7°$. For the spectral distribution of the radiation we take a Gaussian with 0.13-eV FWHM. The calculated energy distribution function $N_{\bar{\vartheta}}(E)$ is plotted in Fig. 9 for six photon energies between 6.2 and 7.8 eV and the three average angles of emission $\bar{\vartheta} = 30°$, $45°$, and $60°$. The scale for $N_{\bar{\vartheta}}(E)$ is in arbitrary units but is the same for all ω and ϑ. Also indicated is the box expected for the energy distribution function of all emitted electrons irrespective of their direction of emission. The width of $N_{\bar{\vartheta}}(E)$ is surprisingly large, it is caused mainly by the finite angular resolution.

The width increases with increasing ω and ϑ until $N_{\bar{3}}(E)$ goes to zero as ϑ_{max} is reached. An example is the truncation of $N_{60^\circ}(E)$ for $\omega > 6.6$ eV.

The energy distribution functions of Fig. 9 do not include the excitation probability which is proportional to $|\langle n\vec{k}|\vec{A}\cdot\vec{p}|n'\vec{k}\rangle|^2$, where $\vec{A}$ is the vector potential of the radiation. The dipole matrix element which is given by Eq. (2) for the NFE case is therefore responsible for the selection rules determining the dependence of the angular resolved photoemission on the polarization of the incident radiation. We discuss this dependence for the $(1\bar{1}0)$ mirror plane as the plane of emission, corresponding to our experiments for $\bar{\vartheta} = 30^\circ$ and 60°. The initial and final states given in Eq. (1) are both even under reflection at this mirror plane in this case, since $\vec{k}$ is restricted to $(1\bar{1}0)$ by $\vec{k}$ conservation. This is not strictly true experimentally because of the finite angular resolution, i.e., $\vec{k}_t$ actually has a small component perpendicular to $(1\bar{1}0)$, but we neglect this minor effect in discussing the polarization dependence. The component of the momentum operator $\vec{p}$ perpendicular to $(1\bar{1}0)$ is odd under reflexion while its component in $(1\bar{1}0)$ is unchanged and thus even. The transition is therefore zero for $\vec{A}$ perpendicular to $(1\bar{1}0)$ but has a finite value for $\vec{A}$ in the mirror plane.[1] The same result is obtained from group theory or, e.g., considering the first term and the six terms with V_{002} and V_{111} on the right-hand side of Eq. (2).
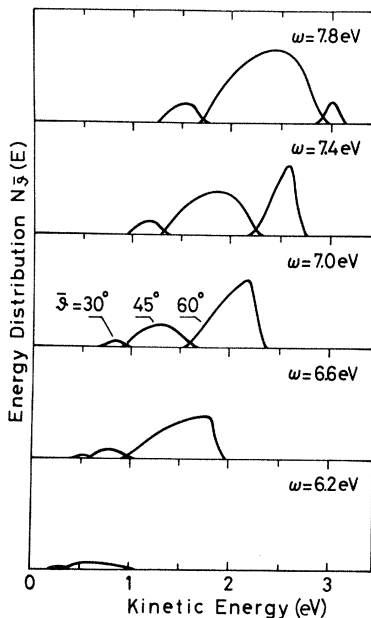

FIG. 10. Angular resolved NFE energy distribution function calculated as previously done for the functions shown in Fig. 9 but including the dependence of the transition probability on the tangential component $\vec{k}_t$ of the wave vector.
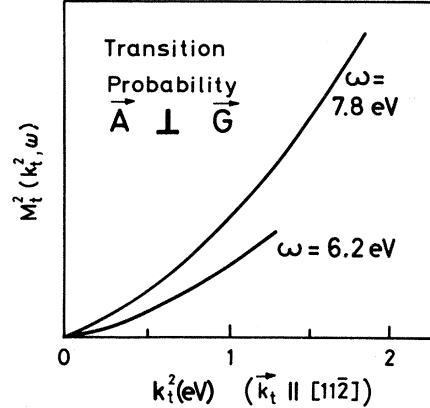

FIG. 11. Dependence of the transition probability, i.e., the tangential component of the dipole matrix element squared, on k_t^2, which is the tangential component of the wave vector squared. This dependence is used to calculate the angular resolved NFE energy distribution functions presented in Fig. 10 from those of Fig. 9.

Since there are the three equivalent mirror planes $(1\bar{1}0)$, $(01\bar{1})$, and $(\bar{1}01)$ intersecting at $[111]$, the transition probability is zero for $\vec{A}$ perpendicular to $[111]$ provided $\vec{k}$ is parallel to this axis and thus common to all three mirror planes.

The selection rules predict a drastic polarization dependence of the elastically emitted photoelectrons: There is no emission into $(1\bar{1}0)$ for $\vec{A}$ perpendicular to this mirror plane. This result is valid beyond the NFE approximation for all cases with both the initial and final states even or odd under reflection at $(1\bar{1}0)$. Furthermore, the transition probability and thus the emission will drastically depend on k_t for $\vec{A}$ parallel to $[11\bar{2}]$ since it vanishes for $\vec{k}_t = 0$. We include the transition probability in $N_{\bar{3}}(E)$ for this orientation of $\vec{A}$ by calculating numerically the contributions of the six terms of Eq. (2) containing V_{200} V_{111}. This is a reasonable approximation since only the pseudopotentials V_{200} and V_{111} tend to be of importance in NFE fcc metals and since the energy denominators increase for higher G_ν. The resulting energy distribution functions presented in Fig. 10 clearly show the dependence of the emission on $\vec{k}_t$. Comparing with Fig. 9, the emission at small angles, i.e., small $\vec{k}_t$ is seen to be strongly suppressed. The actual dependence of the transition probability bility on k_t^2 as shown in Fig. 11 for $\omega = 6.2$ and 7.8 eV turns out to be linear at small values of k_t^2, as expected.

IV. BAND-STRUCTURE ANALYSIS OF THE EXPERIMENTAL RESULTS

The elastic low-energy photoemission from the noble metals originates from transitions between the initial states in the neighborhood of the L_2,

level just below E_F to final states around L_1 above $E_{vac} = E_F + \Phi$.[14] This is apparent for Cu in which case the band structure[11] presented in Fig. 6 is consistent with the detailed piezooptical experiments in the visible and near ultraviolet region, again assuming direct transitions to be responsible for the absorption.[15] For the (111) surface and $\bar{9} = 30°$ and 60° the plane of emission is (1$\bar{1}$0), confining $\vec{k}$ to this plane as discussed in Sec. III. The initial and final states have even parity under a reflection at this plane, i.e., the same selection rules as discussed for the NFE case apply. Comparing the experimental results for Cu(111) (Fig. 4) and Ag(111) (Fig. 5) with the NFE prediction of Fig. 10 we first note the correct sign of the experimental polarization effect. This is, of course, the most compelling evidence in favor of the three-step model. The reversal of the sign in the observed polarization effect for $\bar{9} = 45°$ with (11$\bar{2}$) as the plane of emission confirms the agreement. Although no strict selection rule is valid for this plane, there is an "approximate" selection rule of the same nature since it is enclosed by the (01$\bar{1}$) and ($\bar{1}$01) mirror planes with an angle of enclosure of only ±30°.

The experiments show no polarization effect whatsoever for Cu (110) and (001) surfaces. This again agrees exactly with the three-step model which predicts total internal reflection for these surfaces at low photon energies, using the band structure of Fig. 6. This agreement also validates the assumption that inelastic or incoherent scattering of the excited electrons wipes out the polarization dependence completely since we would observe a residual polarization effect for Cu (110) and (001) surfaces otherwise. The increase of the polarization effect observed for (111) emission with increased surface cleanliness and perfection, i.e., reduced inelastic or incoherent surface scattering further supports this assumption. We therefore identify $N_{\parallel}(E) - N_{\perp}(E)$ with elastic photoemission from Cu and Ag (111) surfaces.

Comparing the experimental results for elastic photoemission from Cu and Ag (111) surfaces as presented in Figs. 4 and 5 with the NFE calculation in Fig. 10, we find the same qualitative trend but no quantitative agreement. This is the result which we anticipated at the beginning of Sec. III. In order to perform a quantitative analysis, we have to start from the actual $E(\vec{k})$ values in the Brillouin zone, not just along special symmetry lines as in Fig. 6. Instead of performing a complete band-structure calculation, we use the combined interpolation scheme developed by Saffren, Ehrenreich, and collaborators, and Mueller[16] with the simplification introduced by Smith and Mattheis.[17] The interpolation scheme is capable of reproducing $E(k)$ as given by a band-structure

calculation at any point in the Brillouin zone once the constants contained in it are adjusted to a few $E(k)$ values at points of high symmetry. Alternatively, the constants may be adjusted to energies derived from experiments. We actually start with the parameters used by Smith and Mattheis and change some of the parameters slightly in order to optimize the agreement with our measurements, and, at the same time, with other independent experimental information, the most important of which is the neck radius. The Fermi energy is recalculated after each change of the constants by adding to the volume of the average Fermi sphere with radius $\bar{k}_F = \frac{1}{3}(k_\Delta + 2k_L)$ the contribution of the necks, approximated by truncated cones, correcting for the spherical segments which were counted twice, and equating the total volume to half the volume of the Brillouin zone. This procedure is similar to the one used by Segall, it is quite accurate since the volume inside of the belly with radii k_Δ along [001] and k_L along [110] is practically identical to the volume of the sphere with radius $\bar{k}_F$ and since the contribution of the necks to the total volume inside of the Fermi surface is small.

The best agreement for Cu(111) is presented in Fig. 12 which gives the contours of constant energies in the (1$\bar{1}$0) plane in the same fashion as for NFE case in Fig. 8. Strong deviations from the
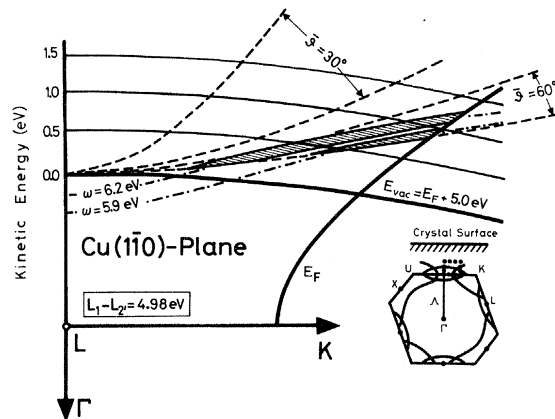

FIG. 12. Contours of constant energy for Cu in the neighborhood of the L point, characterizing direct optical transitions. The plane of the figure is (1$\bar{1}$0). The contours are calculated by means of the combined interpolation scheme (see Refs. 16 and 17), adjusting some of the parameters contained in this scheme to produce the best fit to the experiments of this paper and to piezooptical and de Haas—van Alphen measurements. The figure should be compared to the corresponding Fig. 8 for the hypothetical NFE Cu. The shaded areas are those regions of $\vec{k}$ space which contribute to the signal of the detectors mounted with respect to the surface normal at the angles indicated. The boundaries of these regions are determined by the angular and spectral resolution of ±10° and 0.13-eV FWHM, respectively.

TABLE I. Newly adjusted parameters of the combined interpolation scheme for Cu.

	S (eV)	V_{200} (eV)	A_6 (eV)	$E_F - \Gamma_1$ (eV)	Φ (eV)
This paper	12.69	1.11	0.17	9.30	5.0
Smith[a]	9.99	1.04	0.13		

[a]Reference 17.

NFE case are apparent. As an example the optical energy surfaces $E_{n'}(\vec{k}) = E_n(\vec{k}) = \omega$ are no longer planes perpendicular to [111]. There still is approximate rotational symmetry around the [111] axis, although small deviations show up for large $\vec{k}_t$. To get this fit, we have to change three of the 13 parameters contained in the combined interpolation scheme. We increase the parameter S which incorporates hybridization and orthogonalization effects. At the L point, S influences the positions of the L_1 levels only. We also have to change the tight-binding parameter A_6 which affects the L_3 levels and changes the curvature of the initial states in a way which increases the agreement with our measurements. In addition we change the pseudopotential V_{200} slightly resulting in an even better agreement.

According to the calculation, elastic photoelectrons are first emitted into the $\bar{9} = 60°$ window at about 5.9 eV, whereas elastic emission occurs for 60° and 45° but not for 30° at $\omega = 6.2$ eV. Both facts agree with our experimental results. There is a minor discrepancy for 45° at $\omega = 5.9$ eV. The energy contours predict no elastic emission while Fig. 4 shows some elastic photoelectrons. We attribute this discrepancy to residual contact potentials within the analyzer. It is reassuring, however, that the experiment shows the correct trend in the intensities: The 60° emission is stronger than the 45° emission at 5.9 eV, while these intensities are reversed at 6.2 eV. Another point of agreement is the energy location and the trend in the energy shift of the maximum in the elastic emission. For example, the maximum of of the 60° emission shifts to higher energies with

increasing ω. Similarly, the maximum shifts to higher energies with increasing angle of emission at fixed photon energy as can be seen for $\omega = 6.2$ eV. No attempt is made to estimate the number of states contributing to elastic emission for particular ω and $\bar{9}$ from Fig. 12 since the dependence of the transition probability on k_t drastically influences $N(E)$ as seen for NFE comparing Figs. 9 and 10. The calculation predicts also no elastic emission from (110) and (001) surfaces at low energies since all excited electrons suffer total internal reflection. This explains the lack of any polarization effect in our experiments for these surface orientations.

The constants of the combined interpolation scheme which we have changed and the corresponding constants used by Smith and Mattheiss[17] to fit Burdick's Cu band structure[11] are listed in Table I together with the values for E_F and Φ. The value of the work function Φ is derived from the high-energy cutoff of the different $N_{\bar{3}}(E)$ curves; it is slightly higher than generally reported since we did not use argon-ion bombardment and thus will have some residual oxide at the surface which tends to increase Φ.[18] Table II compares the values of various energy gaps and of the neck radius as calculated in this paper using the combined interpolation scheme with independent piezooptical[15] and de Haas–van Alphen,[19] (dHvA) measurements. The original values calculated by Burdick[11] are also listed.

We obtain the best fit to the elastic emission from Ag(111) as given in Fig. 5 with the energy contours presented in Fig. 13. The contours predict correctly that elastic emission at $\omega = 4.9$ eV

TABLE II. Calculated and measured neck radius and various energy gaps for Cu.

	Neck radius $(\pi/4a)$	$L_1 - E_F$ (eV)	$L_1 - L_{2'}$ (eV)	$E_F - L_3^u$ (eV)[a]	$X_{4'} - X_5$ (eV)
This paper	1.178	4.11	4.98	2.13	4.0
dHvA[b]	1.184				
Piezo-optic[c]		4.15		2.1	4.0
Burdick[d]		3.95	4.56	2.10	3.97

[a]The superscript u refers to the upper L_3 level in the d bands.
[b]Reference 19.
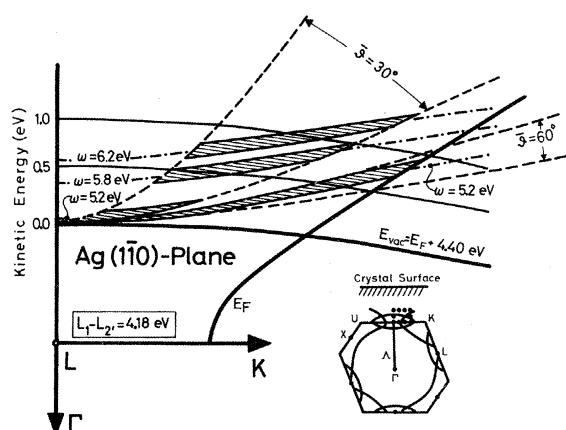[c]Reference 15.
[d]Reference 11.

FIG. 13. Contours of constant energy for Ag in the neighborhood of the L point, characterizing direct optical transitions. The contours are calculated in the same way as the ones presented in Fig. 12 for Cu.

should occur for 60° but not for 30°, whereas elastic emission should be observed for 30° above $\omega = 5.2$ eV. They also contain the observed shift in the maxima of $N_{\bar{3}}(E)$ to higher energies with increasing photon energy and emission angle. Minor discrepancies are the observed elastic emission for 45° at $\omega = 4.9$ eV and for 60° at $\omega > 5.8$ eV which should be zero according to the calculated energy contours. The discrepancies are not serious, however, since the observed signals for 60° at $\omega = 5.8$ and 6.2 eV are barely above the noise and definitely smaller than the corresponding signals for 45° and 30°. Table III contains the adjusted parameters of the combined interpolation scheme together with the Fermi energy and the work function, while our calculation and the calculation by Christensen are compared to independent Fermi surface and optical experiments in Table IV.

V. CONCLUSIONS

The analysis of Sec. IV hinges on the validity of the three-step model. In particular, we use the angular dependence of the dipole matrix element describing direct transitions and the conservation of the tangential vector $\vec{k}_t$ which is the reduced wave vector in the surface plane during emission to identify photoelectrons elastically emitted from

(111) surfaces. There are several facts which support the validity of the model for transitions between s-p bands, i.e., in the spectral range below 6.2 eV: It predicts the observed *sign* of the polarization effect for (111) emission, i.e., the dependence on the polarization of the incident radiation, it also explains the lack of elastic emission from (110) and (001) surfaces, and it leads to a band structure consistent with the experiments of this paper as well as with the results of independent optical and dHvA measurements.

The consistency of a model describing photoemission with independent optical and transport investigations is an obvious requirement, and one of the most serious objections against attempts to describe photoemission from d band metals in terms of nondirect transitions[14,24] is that this concept does not explain the piezooptical results.[15] In fact the consistency with the various different experiments justifies the claim that our set of parameters for the combined interpolation scheme results in the most reliable $E(k)$ values available for Cu and Ag. The uncertainty of ± 0.1 eV for states about 6 eV above the Fermi energy is mainly caused by the uncertainty in the determination of the work function. For a fixed value of the work function there is virtually only one set of parameters for the combined interpolation scheme which produced the consistency mentioned above.

In principle, the momentum distribution probes the various individual transitions directly, although we have to take the finite angular resolution into account. This is the reason for the high spectroscopic accuracy of our analysis, since the important interaction between the sp and the d states is particularly strong for the final states around the L point which are responsible for the elastic photoemission from Cu and Ag (111) surfaces at low energies. Thus our measurements probe this interaction directly, while it is particularly difficult to calculate it from first principles. Another feature of the momentum distribution is worth mentioning. Since its analysis gives the functional dependence $E(k)$ of the states involved, it supplies more-detailed information than other optical measurements which characteristically supply energy gaps at critical points in the Brillouin zone. For example, it is not possible to explain the observed momentum distribution using a k^2 expansion of

TABLE III. Newly adjusted parameters of the combined interpolation scheme for Ag.

	S (eV)	B_g (eV)	V_{111} (eV)	E_0 (eV)	$E_F - \Gamma_1$ (eV)	Φ (eV)
This paper	14.69	10.61	0.50	1.19	7.23	4.4
Smith[a]	11.22	12.77	0.59	-0.007		

[a]Reference 17.

TABLE IV. Calculated and measured neck radius and various energy gaps for Ag.

	Neck radius	$L_1 - E_F$ (eV)	$L_1 - L_{2'}$ (eV)	$E_F - L_3^u$ (eV)[a]	$X_{4'} - X_5$ (eV)
This paper	0.857	3.89	4.18	3.98	5.56
dHvA[b]	0.853				
Optical		3.85[c]	4.16[c,d]	3.99[c]	
Christensen[e]		3.33	3.49	3.97	5.75

[a]The superscript u refers to the upper L_3 level in the d bands.
[b]Reference 20.
[c]Reference 21.
[d]Reference 22.
[e]Reference 23.

$E(k)$ around the L point while such an effective mas mass expansion will still produce the singularity in the joint density of states at $\omega = L_1 - L_2$, observed piezooptically.[15] The structure observed in the thermomodulated spectra[21] is another case in point. In fact, the effective mass expansion used to fit these spectra fails to predict the strong $45°$ emission which we observe at $\omega = 5.8$ and 6.2 eV for Ag(111), i.e., for emission originating from states with k_t about twice the neck radius.

Any photoemission experiments is likely to produce a sizeable fraction of scattered photoelectrons in addition to the elastic emission. The situation is quite similar to the LEED case where the elastically reflected electrons are routinely filtered out electrostatically. In fact the Laue spots of the LEED pattern are an example for our definition of elastic reflection or emission, i.e., coherent scattering at the periodic potential in the volume or at the surface. We found the ratio of elastic emission to the emission of incoherently scattered electrons to increase drastically with increasing surface perfection. Thus a large fraction of the scattering occurs at irregularities of the surface. Since our analysis is based on the truly elastic photoemission only, it is not influenced by incoherent scattering, provided these scattering processes average out any dependence on the polarization of the radiation at normal incidence. This is indeed the case, as evidenced by the lack of any polarization effect for emission from (110) and (001) Cu surfaces in the spectral range below 6.2 eV. The three-step model predicts no elastic emission in these cases, and the scattered electrons which are emitted no longer show a polarization anisotropy.

Some of the incoherent scattering processes will change mainly the momentum of the excited electrons, with little or no change in energy. While these quasielastically emitted electrons do not contribute to the polarization-dependent momentum distribution, they cannot be separated from the truly elastic emission in the conventional angular integrated energy distribution functions. This is another advantage of the measurements presented here compared to conventional photoemission.

The three-step model does not contain the influence of the surface on the electronic states, i.e., it describes the excitation as transitions between Bloch states. The consistency of our measurements with independent optical and dHvA results shows that this influence is not important numerically in the low-energy spectral region. Such an influence might be more pronounced at higher energies where the escape depth of the photoelectrons is smaller. Similarly, many-body effects as proposed by Doniach[25] require excitation from flat bands, their importance can thus be tested only at higher photon energies for which excitations from d bands contribute to the photoemission from Cu and Ag. As another consequence of the present investigation, more sophisticated theories of the photoemission process[26] must recover the predictions of the three-step model at least for the low-energy spectral region.

ACKNOWLEDGMENTS

[1]G. W. Gobeli, F. G. Allen, and E. O. Kane, Phys. Rev. Lett. 12, 94 (1964); E. O. Kane, ibid. 12, 97 (1964).
[2]Preliminary results for Cu were reported by U. Gerhardt and E. Dietz [Phys. Rev. Lett. 26, 1477 (1971)]
and by I. Lindau and S. B. M. Hagström [J. Phys. E 4, 936 (1971)]. Some of the papers on other materials are T. Gustafsson, P. O. Nielsson, and L. Walldén, Phys. Lett. A 37, 121 (1971); A. Sugaya and S. Kawaji, Jpn. J. Appl. Phys. 11, 909 (1972); B. Feuerbacher, and B. Fitton, Phys. Rev. Lett. 30, 923 (1973); N. V. Smith and M. M. Traum, ibid. 31, 1247 (1973); M. M. Traum, N. V. Smith, and F. J. Di Salvo, ibid. 32,

1241 (1974); B. Feuerbacher and B. Fitton, Solid State Commun. 15, 301 (1974); B. Feuerbacher and N. E. Christensen, Phys. Rev. B 10, 2373 (1974).

[3]H. Thomas, Z. Phys. 147, 395 (1957); H. Mayer and H. Thomas, ibid. 147, 419 (1957); S. Methfessel, ibid. 147, 442 (1957).

[4]I. Tamm and S. Schubin, Z. Phys. 68, 97 (1931); H. Fröhlich, ibid. 75, 539 (1932); K. Mitchell, Proc. R. Soc. A 146, 422 (1934).

[5]One more recent publication on the subject is by S. A. Flodström and J. G. Endriz, Phys. Rev. Lett. 31, 893 (1973). It gives the measured yield ratio for polarization parallel and perpendicular to the plane of incidence as a function of the angle of incidence for Al. The measured ratio is compared to the one calculated from an "isotropic-volume-photoeffect theory," which unfortunately neglects the polarization dependence of the elastic photoemission, i.e., the angular dependence of the transition matrix element. Taking this polarization dependence into account, we arrive at much higher values for the yield ratio. For Al at $h\nu = 5.4$ eV and $\vartheta = 45°$, we calculate $Y_p/Y_s = 2.6$, assuming transverse electromagnetic waves in the metal only, i.e., validity of the conventional Fresnel equations. The corresponding ratios measured and calculated by Flodström and Endriz are ~ 4.7 and ~ 1.9, respectively. The problem is of course how to include the longitudinal wave which is also present in the metal. Although the inclusion of the longitudinal wave is likely to further increase the yield ratio, we do not know how to treat this problem properly.

[6]B. J. Waclawski and E. W. Plummer, Phys. Rev. Lett. 29, 783 (1972); B. Feuerbacher and B. Fitton, ibid. 29, 786 (1972).

[7]H. Kanter, Phys. Rev. B 1, 522 (1970).

[8]This polarizer is manufactured by Polacoat, Inc., 9750 Conklin Rd., Blue Ash, Ohio 45242.

[9]H. Becker, E. Dietz, and U. Gerhardt, Rev. Sci. Instrum. 43, 1587 (1972); U. Gerhardt, ibid. 44, 657 (1973).

[10]W. T. Tegart, The Electrolytic and Chemical Polishing of Metals, 2nd ed. (Pergamon, New York, 1959).

[11]B. Segall, Phys. Rev. 125, 109 (1962); G. A. Burdick, ibid. 129, 138 (1963).

[12]G. D. Mahan, Phys. Rev. Lett. 24, 1068 (1970); G. D. Mahan, Phys. Rev. B 2, 4334 (1970).

[13]R. Y. Koyama and N. V. Smith, Phys. Rev. B 2, 3049 (1970).

[14]C. N. Berglund and W. E. Spicer, Phys. Rev. 136, A1030 (1964); 136, A1044 (1964).

[15]U. Gerhardt, Phys. Rev. 172, 651 (1968).

[16]M. Saffren, in The Fermi Surface, edited by W. A. Harrison and M. B. Webb (Wiley, New York, 1960), p. 341; L. Hodges and H. Ehrenreich, Phys. Rev. Lett. 10, 203 (1965); L. Hodges, H. Ehrenreich, and N. D. Lang, Phys. Rev. 152, 505 (1966); F. M. Mueller, ibid. 153, 659 (1967).

[17]N. V. Smith and L. F. Mattheiss, Phys. Rev. B 9, 1341 (1974).

[18]A. H. Sommer, Photoemissive Materials (Wiley, New York, 1968), p. 27.

[19]W. J. O'Sullivan, A. C. Switendick, and J. E. Schirber, Phys. Rev. B 1, 1443 (1970).

[20]J. P. Jan and I. M. Templeton, Phys. Rev. 161, 556 (1967).

[21]R. Rosei, C. H. Culp, and J. H. Weaver, Phys. Rev. B 10, 484 (1974).

[22]Virtually the same value was given earlier by C. E. Morris and D. W. Lynch [Phys. Rev. 182, 719 (1969)] and by L. Wallden and T. Gustafsson [Phys. Scripta 6, 73 (1972)].

[23]N. E. Christensen, Phys. Status Solidi B 54, 551 (1972).

[24]W. E. Spicer, Phys. Rev. Lett. 11, 243 (1963); Phys. Rev. 154, 385 (1967); W. F. Krolikowski and W. E. Spicer, ibid. 185, 882 (1969).

[25]S. Doniach, Phys. Rev. B 2, 3898 (1970).

[26]G. D. Mahan, Phys. Rev. B 2, 4334 (1970); W. L. Schaich and N. W. Ashcroft, ibid. 3, 2452 (1971).